Solar RRL
www.solar-rrl.com

Cu(II) and Ni(II) Phthalocyanine-Based Hole-Transporting Materials for Stable Perovskite Solar Cells with Efficiencies Reaching 20.0%

Jianxing Xia, Jorge Labella, Perihan Kübra Demircioglu, Manuel Pérez-Escribano, Joaquín Calbo, Abdullah M. Asiri, Enrique Ortí, Mine Ince,* Mohammad Khaja Nazeeruddin,* and Tomás Torres**

Herein, Cu(II)Pcs and Ni(II)Pcs peripherally tetra-functionalized with 5-hexylthiophene (HT), 5-hexyl-2,2′-bithiophene (HBT), and tertbutyl groups (TB) are readily synthesized and employed as hole-transporting materials (HTMs) in mixed-ion perovskite ($[FAPbI_3]_{0.85}[MAPbBr_3]_{0.15}$) solar cells, achieving power conversion efficiencies (PCEs) up to 20.0%. Remarkably, both the peripheral functionalization and the central metal are found to play a role in the performance. Through a combination of experimental and theoretical techniques, it is found that the simplest HTM, TB-CuPc, is the best-performing HTM primarily due to its higher hole mobility and a more appropriate highest-occupied molecular orbital, whose enables efficient hole extraction without open-circuit voltage (V_{oc})losses. This derivative leads to PCEs of 19.96%, which are among the highest values for Pc-based HTMs. Importantly, devices incorporating these HTMs present significantly higher stability compared to those based on spiro-OMeTAD. The results here presented pave the way for more realistic, efficient, and inexpensive photovoltaic devices using phthalocyanine derivatives.

1. Introduction

Perovskite solar cells (PSCs) continue to be a central topic in state-of-the-art photovoltaic research due to their facile, low-cost fabrication process, and rapidly improved power conversion efficiency (PCE).[1–3] PSCs are generally classified into two device configurations according to the way the functional layers are stacked: conventional (n-i-p) and inverted (p-i-n).[1] During the past years, inverted (p-i-n) devices have attracted significant attention owing to their multiple advantages, such as better device stability, negligible hysteresis, and versatile implementation in tandem devices.[4] Nevertheless, many researchers are still focused on conventional (n-i-p) devices as they provide the highest efficiencies, reaching impressive values exceeding 25%.[5] In (n-i-p)

J. Xia, M. K. Nazeeruddin
Institute of Molecular Plus
Tianjin University
Tianjin 300072, China
E-mail: mdkhaja.nazeeruddin@epfl.ch

J. Xia, M. K. Nazeeruddin
Institute of Chemical Sciences and Engineering
École Polytechnique Fedérale de Lausanne (EPFL)
1015 Lausanne, Switzerland

J. Labella, T. Torres
Department of Organic Chemistry
Autónoma University of Madrid
Cantoblanco, 28049 Madrid, Spain
E-mail: tomas.torres@uam.es

P. K. Demircioglu
Department of Natural and Mathematical Sciences
Faculty of Engineering
Tarsus University
33480 Mersin, Turkey

The ORCID identification number(s) for the author(s) of this article can be found under https://doi.org/10.1002/solr.202400371.

DOI: 10.1002/solr.202400371

M. Pérez-Escribano, J. Calbo, E. Ortí
Instituto de Ciencia Molecular
Universidad de Valencia
Catedrático José Beltrán 2, 46980 Paterna, Spain
E-mail: enrique.orti@uv.es

M. Ince
Advanced Technology Research & Application Center
Mersin University
Ciftlikkoy Campus, TR-33343 Mersin, Turkey
E-mail: mine.ince@tarsus.edu.tr

T. Torres
Institute for Advanced Research in Chemical Sciences
Autónoma University of Madrid
Cantoblanco, 28049 Madrid, Spain

T. Torres
IMDEA-Nanociencia
28049 Madrid, Spain

A. M. Asiri
Center of Excellence for Advanced Materials Research (CEAMR)
King Abdulaziz University
P.O. Box 80203, Jeddah 21589, Saudi Arabia

structures, the perovskite layer is sandwiched between an electron-transport layer (ETL, n-type) and a hole-transport layer (HTL, p-type), which ensures selective charge blocking and extraction.[6–8] The electron-transport materials (ETMs) are mainly monopolized by mesoporous or planar metal oxides, such as TiO_2, which is the most used ETM due to its excellent performance and easy processability.[7,9] In contrast, the hole-transporting materials (HTMs) have been explored in more detail and multiple chemical derivatives of different structures and natures (e.g., classical semiconducting polymers or small molecules) have been postulated.[10] Among them, 2,2′,7,7′-tetrakis (*N*,*N*-di-p-methoxyphenylamine)-9,9′-spirobifluorene (spiro-OMeTAD)[11] and poly(triaryl-amine) (PTAA)[12] hold a privileged position. However, spiro-OMeTAD and PTAA, although efficient, present major drawbacks in the form of elevated production costs and insufficient long-term stabilities, which constitute a serious problem for large-scale applications. Therefore, the search for stable and economic HTMs is still an urgent need for the further development of (n-i-p) PSCs.

Phthalocyanines (Pcs),[13] square-planar, 18 π-electrons, aromatic macrocycles consisting of four diiminoisoindoles, are p-type semiconductors widely employed as electroactive components in molecular photovoltaics.[14–16] Due to their extended planar core, they present a strong tendency to aggregate into π-stacked structures, which results in efficient intermolecular π–π overlap and improved semiconducting properties.[17] This, together with their numerous advantageous properties such as structural robustness, attractive optical absorption and emission, strong aromaticity, and rich coordination chemistry, spurred the application of Pcs as hole-injectors in dye-sensitized solar cells[18] and as donor materials in organic solar cells.[19] More recently, Pcs have also emerged as promising HTMs in PSCs due to the chemical versatility inherent to the macrocycle.[20] This enables the synthesis of meticulously designed HTMs with tailored properties such as suitable highest-occupied molecular orbital (HOMO) energy levels for efficient hole extraction from perovskites, enhanced stability, hole mobility, and self-assembly behavior. To optimize these properties, significant attention has been directed toward modulating the electron-donating characteristics of the peripheral groups of Pcs, since they directly influence the π-system. Thus, various chemical groups, including alkyl or alkyloxy chains, arylamine moieties, and heterocycles, have been employed as peripheral substituents in Pc-based HTMs.[20] In this context, Zn(II)Pcs have been more explored due to their higher PCEs. In contrast, the evolution of HTMs composed of Pcs hosting other metals, such as Cu(II) and Ni(II), has progressed slower, despite their highly beneficial attributes, including higher coordination chemical stability and excellent electron transfer kinetics.[21–25] In a pivotal study conducted by our research groups, the photovoltaic performance of Zn(II)Pcs peripherally functionalized with tert-butyl (TB-ZnPc), 5-hexylthiophene (HT-ZnPc), or 5-hexyl-2,2′-bithiophene (HBT-ZnPc) groups, was evaluated.[26] Notably, PCEs of up to 17.5% were achieved, rivaling those obtained with spiro-OMeTAD. Importantly, the aforementioned peripheral functionalization is readily accessible from a synthetic standpoint and provides excellent solubility, resulting in notably high fill factor (FF) values, alongside excellent thin-film morphologies and conductivities. These valuable attributes make Cu(II)Pcs and Ni(II)Pcs equipped with TB, HT, and HBT groups promising candidates as HTMs.

In this work, we synthesized six different Cu(II) and Ni(II)Pcs equipped with TB, HT, and HBT peripheral groups (**Figure 1**), with the aim of probing their capabilities as efficient, stable, and low-cost HTMs. Although these six HTMs showed excellent performance, the simplest Pcs (**TB-CuPc** and **TB-NiPcs**) outperformed the more complex thiophene-based analogs. As supported by theoretical calculations and several experimental techniques, the origin of this finding arises, on the one hand, from losses in the open-circuit voltage (V_{oc}) stemming from the HOMO destabilization upon including thiophene moieties, and on the other hand, from the lower hole mobility found for the thiophene-containing Pcs, possibly due to less robust π–π packing. Moreover, it is observed that Cu(II)Pc-based HTMs lead to higher PCEs compared to Ni(II)Pc-based HTMs, once again due to the larger V_{oc} values and hole mobilities. Our results underscore the crucial role of both the peripheral groups and the central metal in the performance of Pc-based HTMs, as both control

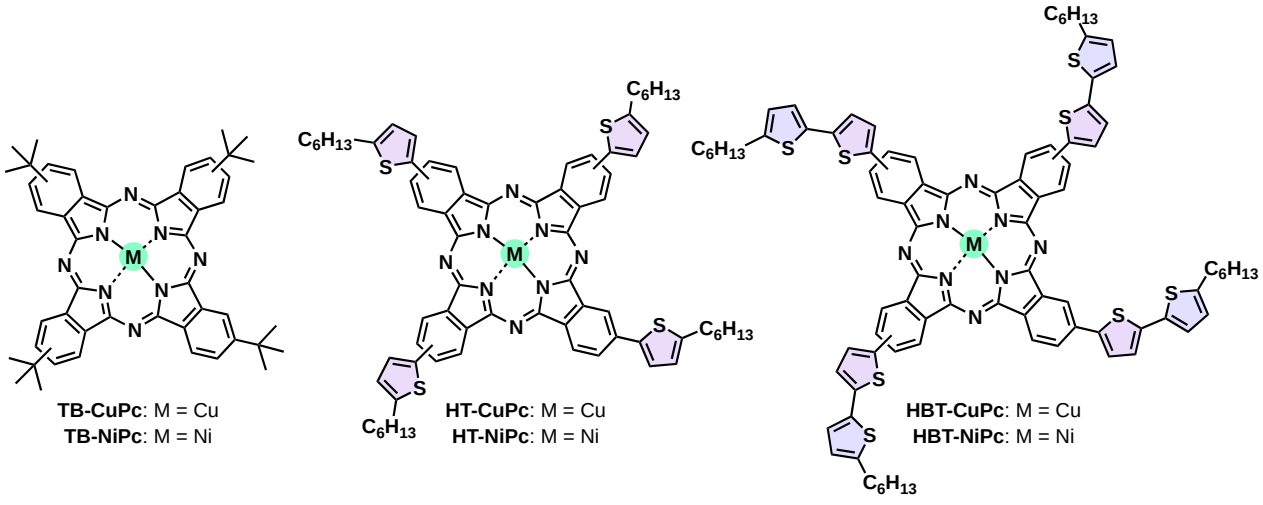

Figure 1. Molecular structures of **TB-MPc**, **HT-MPc**, and **HBT-MPc,** being M = Cu or Ni.

the molecular structure, organization, and electronic properties, key aspects for efficiently extracting and transporting holes from the perovskite. Importantly, we also demonstrate that the insertion of these HTMs significantly improves stability in comparison to spiro-OMeTAD, which is key for realistic applications.

2. Results and Discussion

2.1. Synthesis and Molecular Structure

Tetra-5-hexylthiophene (HT) and tetra-tertbutyl (TB) substituted Ni(II)Pcs and Cu(II)Pcs were prepared according to the previously published procedure,[26] which is based on the general cyclotetramerization reaction of the corresponding phthalonitriles in the presence of metal salts in dimethylethanolamine (DMAE). The tetra-5-hexyl-2,2′-bithiophene-substituted NiPc and CuPc (HBT-MPCs) were prepared via Suzuki cross-coupling reaction between the corresponding tetraiodo-substituted MPc and the hexylbithiophene-boronic acid pinacol ester by modification of the previously published procedure,[26] in which Ni or Cu metals were incorporated inside the macrocycle (further experimental details are provided in the SI).

To visualize the structural differences between **HT-MPcs** and **HTB-MPcs**, density functional theory (DFT) calculations were performed at the BMK/LANL2DZ+6-31G(d,p) level of theory (see the Supporting Information for full computational details). **Figure 2** shows the minimum-energy optimized structures calculated for **TB-CuPc** and **HBT-CuPc** as illustrative examples (see Figure S15, Supporting Information, for unsubstituted **CuPc** and **HT-CuPc**). The Pc core remains planar and mainly symmetric in all systems. Deviations from planarity are associated with the introduction of the thienyl peripheral substituents and are quantified by the dihedral angles formed between the isoindole Pc units and the attached thiophene ring in both **HT-MPcs** and **HTB-MPcs** (angle α) and between the thiophene rings in **HTB-MPcs** (angle β). Angle α has values around 21.5° whereas β lies in the 9–12° range, with no significant difference being found between CuPcs and NiPcs (Table S1, Supporting Information). These results highlight the reduced influence of the metal cation in the structure of the proposed MPcs. The small values found for both α and β dihedral angles indicate that the π–π stacking capability of the Pc core is not significantly reduced in **HT-MPcs** and **HTB-MPcs**, and hence would maintain the hole-transport properties of these systems.

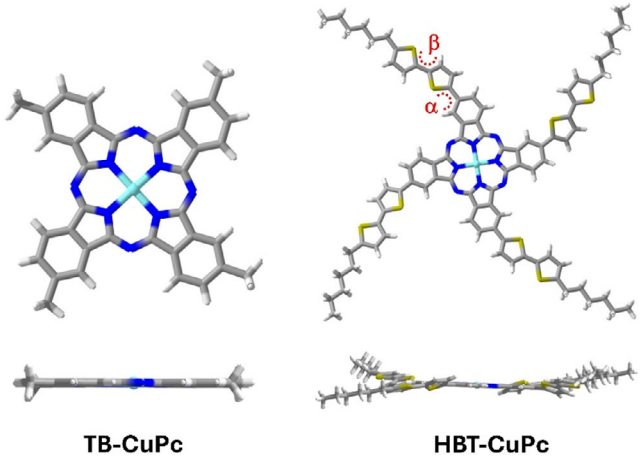

Figure 2. Top and side views of the BMK/LANL2DZ+6-31G(d,p) minimum-energy optimized structures computed for **TB-CuPc** and **HBT-CuPc** in THF. The α and β rotation dihedral angles are marked in red.

2.2. Optical and Electrochemical Properties

The optical properties of the MPcs were studied by measuring their absorption spectra in tetrahydrofuran (THF) (**Figure 3** and **Table 1**). **TB-MPcs**, both for Cu and Ni, exhibit sharp Q bands with an absorption maximum at ≈670 nm. The attachment of thiophene units in **HT-CuPc** and **HT-NiPc** produces a less-intense and red-shifted Q absorption in comparison to that of the tertbutyl-substituted Pcs, with maxima at 700 and 694 nm, respectively. A remarkable reduction in the intensity and broadening of the Q-band absorption is observed for **HBT-MPcs**, functionalized with bithiophene units, together with additional absorption features in the range between 400 and 550 nm.

To shed light on the nature of the different excitations that shape the absorption spectrum of the MPcs, the spectra were calculated at the TD-DFT BMK/LANL2DZ+6-31G(d,p) level of theory in THF. The theoretical spectra, which reproduce very well the shape of the experimental spectra (Figure S16, Supporting Information), were further analyzed by computing the natural transition orbitals for the excited states involved in the spectra (Figure S17–S24, Supporting Information). For all MPcs, the Q band arises from either the transitions to the first two singlet excited states (S_1 and S_2) for NiPcs or to the first two doublet excited states (D_1 and D_2) for CuPcs. The transitions appear to be almost degenerate in energy due to the molecular symmetry and show a small influence of the thiophene substituents for **HT-** and **HBT-MPcs**. This remarks the local character of the transitions, which mainly correspond to the HOMO→lowest-unoccupied molecular orbital (LUMO) and LUMO +1 excitations centered in the Pc core. For **TB-MPcs**, the spectral features coincide with those of the unsubstituted **MPc** analogs, with high-lying excited states (mainly S_{14}/S_{15} and D_{13}/D_{14} for

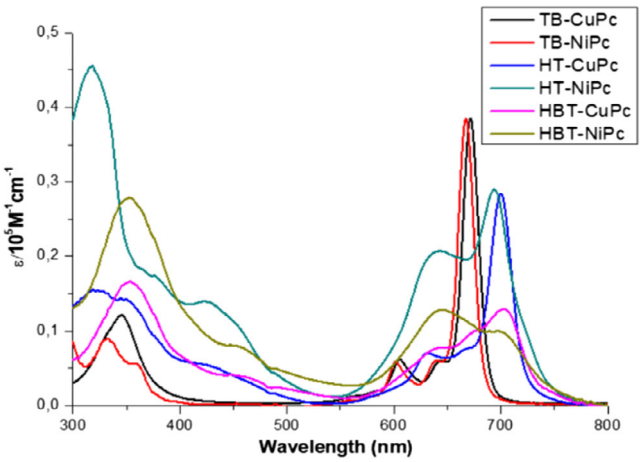

Figure 3. UV–vis absorption spectra of **TB-Cu/NiPcs**, **HT-Cu/NiPcs**, and **HBT-Cu/NiPcs** in THF (10^{-5} M).

Table 1. Experimentally determined optical and electrochemical characteristics of the MPc derivatives.

HTM	λ_{max} [nm]	E_{0-0} [nm]	E_{0-0} [a)] [eV]	E_{ox} [b)] [V]	E_{HOMO} [c)] [eV]	E_{LUMO} [d)] [eV]
TB-CuPc	671	677	1.83	0.83	−5.28	−3.44
TB-NiPc	667	669	1.85	0.89	−5.33	−3.48
HT-CuPc	700	702	1.77	0.50	−4.94	−3.17
HT-NiPc	694	706	1.76	0.53	−4.97	−3.21
HBT-CuPc	703	709	1.75	0.45	−4.89	−3.14
HBT-NiPc	700	707	1.75	0.49	−4.93	−3.18

[a)]Zero–zero excitation energy obtained from the intersection between the normalized absorption and emission spectra;[30] [b)]Versus NHE; [c)]$E_{HOMO} = E_{ox} + 4.44$ (eV).[26] [d)]$E_{LUMO} = E_{HOMO} + E_{0-0}$.

TB-NiPc and **TB-CuPc**, respectively) being responsible for the band around 300 nm, also with local Pc character (Figure S17–S20, Supporting Information). In contrast, the absorption features observed in the range between 300 and 500 nm for **HT-MPcs** and **HBT-MPcs** are mainly due to charge-transfer excitations involving the thiophene substituents and the Pc core, including both thiophene→core and core→thiophene transitions (Figure S21–S24, Supporting Information). This showcases the influence the thiophene peripheral substitution has on the optical properties of the MPcs, as it increases the absorption capabilities in the visible range of the electronic spectrum. Theoretical calculations also reproduce nicely the red-shift experienced by the Q band upon thiophene functionalization, which correlates with the calculated HOMO-LUMO gap trend: 2.18 and 2.20 eV for **TB-Cu/NiPc**, 2.06 and 2.08 eV for **HT-Cu/NiPc**, and 1.98 and 2.00 eV for **HBT-Cu/NiPc**, respectively.

The HOMO energy levels of the proposed MPcs were determined by cyclic voltammetry in combination with differential pulse voltammetry in THF solution (Figure S11–S13, Supporting Information). Fc/Fc^+ was used as the internal standard for all measurements and the potentials were converted to the normal hydrogen electrode (NHE) by the addition of 0.7 V. The electrochemical characteristics of the MPc derivatives are summarized in Table 1 together with the optical absorption properties. The HOMO energy levels of all MPc derivatives align well with the energy levels of the selected perovskite used to build up the PSC devices (as schematically shown in **Figure 4**). This has been proven to be beneficial for hole extraction and to avoid charge recombination.[27,28] When the HTMs are compared, NiPc derivatives show slightly lower HOMO energies (higher oxidation potentials) than CuPcs, in agreement with the theoretical values predicted by DFT calculations (Table S2, Supporting Information). The electron-donating ability of the thiophene units increases the HOMO energy of **HT-MPcs** and **HTB-MPcs** compared to the tertbutyl-substituted **TB-MPcs** derivatives, and results in narrower bandgaps (Table 1). The low-lying HOMO energy levels of **TB-MPcs** may result in higher V_{oc} values compared to those containing thiophene side chains. The frontier molecular orbitals, shown in **Figure 5** for NiPcs, highlight the almost negligible contribution of the thienyl substituents to the HOMO and LUMO levels.

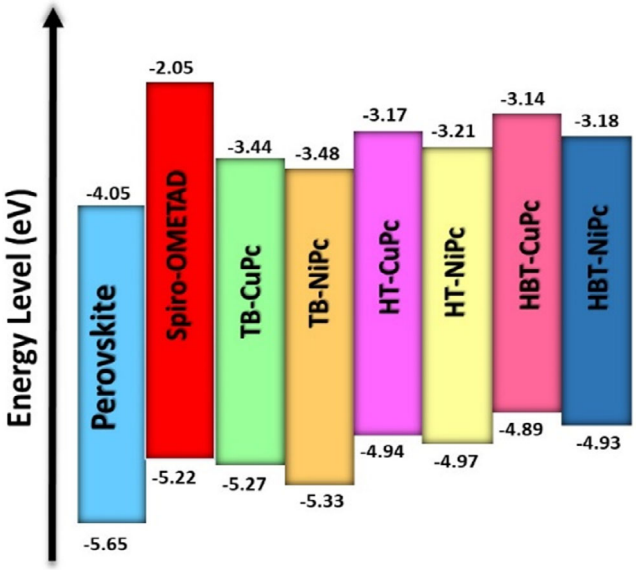

Figure 4. Energy band diagram of the MPc-based HTMs.

The influence of the metal center and the peripheral substituents on the donor ability of MPcs was further investigated by calculating the adiabatic ionization energies (Table S3, Supporting Information) and the spin density (shown in Figure S26, Supporting Information). Oxidation occurs in the Pc core as no spin density is delocalized over the thiophene chains neither for **HT-MPcs** nor for **HBT-MPcs**. Moreover, the contribution of metal pure *d* orbitals in the oxidation is negligible as they lie deep in energy. Thus, the ionization energies are calculated in all cases very similar and close to 5 eV in THF, regardless of whether the metal cation or the substitution pattern is changed.

The hole drift mobility was measured in hole-only devices with the space-charge-limited-current (SCLC) method, with a structure of FTO/PEDOT:PSS/HTM/Au (Figure S14, Supporting Information). As a result, the hole mobility of **TB-CuPc**, **HT-CuPc**, **HBT-CuPc**, **TB-NiPc**, **HT-NiPc**, and **HBT-NiPc** is 6.55×10^{-4}, 5.49×10^{-4}, 3.44×10^{-4}, 5.14×10^{-4}, 4.73×10^{-4}, and 2.23×10^{-4} $cm^2 V^{-1} s^{-1}$, respectively. The results indicate that, for the same metal center, the hole mobility is decreased upon the addition of thiophene substituents (**TB-** to **HT-MPcs**) and when the thiophene chains are further enlarged (**HT-** to **HBT-MPcs**). This might be due to a more impeded π–π aggregation of the molecules in the amorphous film, arising from side-chain torsions, as predicted by the DFT-optimized structures. When the hole mobility is compared within the same molecular scaffold but varying the metal center, Cu-Pcs show slightly higher values. Within the frame of Marcus transport theory,[29] the hole transfer rate (and hence the hole mobility) increases if the hole reorganization energy decreases and the electronic couplings between pairs of monomers in the thin film are larger. The internal gas-phase hole reorganization energies were estimated by means of DFT calculations (see the Supporting Information for details). The values predicted (**Table 2**) are in good agreement with the experimental trends since larger reorganization energies are obtained upon

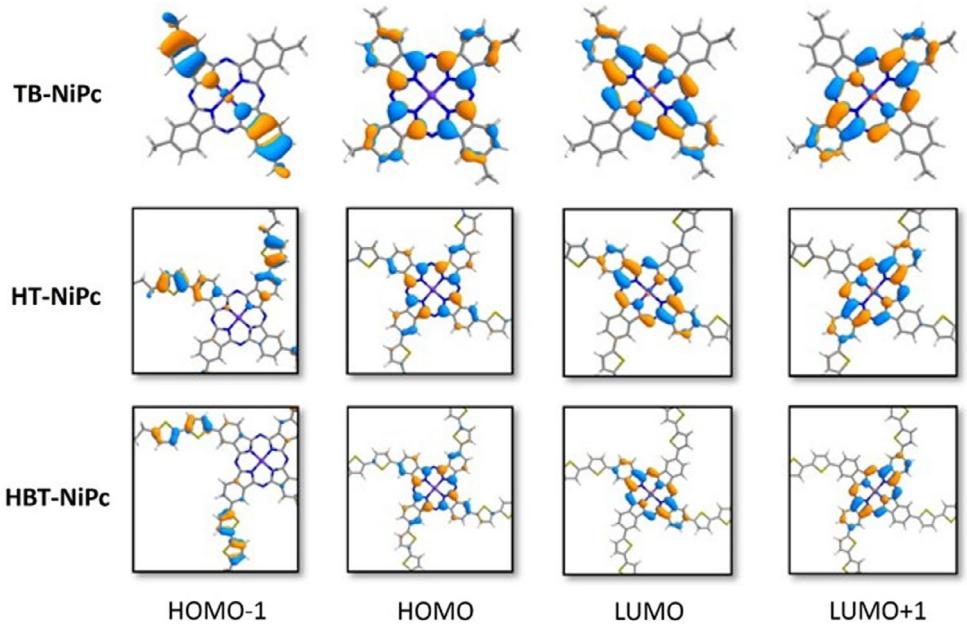

Figure 5. BMK/LANL2DZ+6-31G(d,p) frontier molecular orbitals computed for NiPcs at their minimum-energy structures in THF. Rendering isovalue: 0.03. For **HT-NiPc** and **HBT-NiPc**, the orbitals are zoomed for clarity.

Table 2. BMK/LANL2DZ+6-31G(d,p) internal gas-phase hole reorganization energies (in meV) for all MPcs.

	M-Pc	M-TB	M-HT	M-HBT
Cu	46	47	79	97
Ni	47	49	80	99

peripheral substitution of the MPcs and when replacing Cu with Ni in MPcs. It is noteworthy that the reorganization energies obtained for the MPcs, which are in the range of 50–100 meV, are significantly smaller than those obtained for spiro-OMeTAD at the same level of theory (300 meV). Regarding the electronic couplings, a higher value was obtained for the most interacting dimer of **TB-CuPc** (255 meV) compared to that of **HT-CuPc** (213 meV) and **HBT-CuPc** (145 meV) —these structures resulted from an automated docking and optimization procedure (see the Supporting Information for details). Both the gas-phase hole reorganization energy and the electronic couplings therefore support the hole mobility data recorded experimentally for the family of Pc-based HTMs.

2.3. Photovoltaic Performance

To analyze the performance of **TB-CuPc**, **HT-CuPc**, **HBT-CuPc**, **TB-NiPc**, **HT-NiPc**, and **HBT-NiPc** as HTMs, we fabricated (n-i-p) PSCs using the FTO/C-TiO_2/SnO_2/PCBM/perovskite/HTMs/Au device architecture (**Figure 6**a), a configuration well established in our laboratories. The perovskite absorber ($[FAPbI_3]_{0.85}[MAPbBr_3]_{0.15}$) was sandwiched between C-TiO_2/SnO_2/PCBM layers as the ETMs, and the MPcs served as the HTMs (Figure 6a). The ETL was fabricated following a procedure previously optimized by some of us (see the Supporting Information for further details), and the HTMs were spin-coated onto the top of the perovskite film using chlorobenzene solutions. Small amounts of dopants were added to both the MPcs and spiro-OMeTAD to enhance their conductivity (see the Supporting Information for further details). Reference PSCs were also fabricated using spiro-OMeTAD as the HTM. Finally, a 70 nm thick layer of gold was deposited on top of the HTM, completing the solar cell configuration. As depicted in Figure 6a, cross-section scanning electron microscopy (SEM) revealed good contact at the perovskite/HTM interface, with the thickness of the HTM film deposited onto the perovskite layer measuring ≈50 nm. The width of the perovskite layer in the device was ≈600 nm, a dimension beneficial for efficient PSC fabrication.

Current−voltage ($J-V$) characteristics of the champion devices are presented in Figure 6b, and their corresponding photovoltaic parameters are summarized in **Table 3**. Spin-coating deposition of the **TB-CuPc** HTM results in a PCE of 19.96% with an open-circuit voltage (V_{oc}) of 1.094 V, a short-circuit current density (J_{sc}) of 23.01 mA cm^{-2}, and a FF of 79.3%. However, when the Cu is replaced by the Ni as a central metal, the V_{oc}, FF, and J_{sc} decrease (22.82 mA cm^{-2}, 1.084 V, and 0.786, respectively), resulting in a lower PCE of 19.44%. This result indicates that Cu as a central metal performs better than Ni in **TB-MPcs**, consistent with previously reported trends.[20] In contrast, when thienyl groups are employed as peripheral substituents instead of tertbutyls, the PCE of both **HT-CuPc** and **HT-NiPc** decreases to 19.45 and 18.28%, respectively, with a loss of V_{oc}. The loss of V_{oc} can be attributed to the increase in the HOMO energy level induced by replacing the TB groups with HT moieties, as supported by electrochemical measurements and DFT calculations.

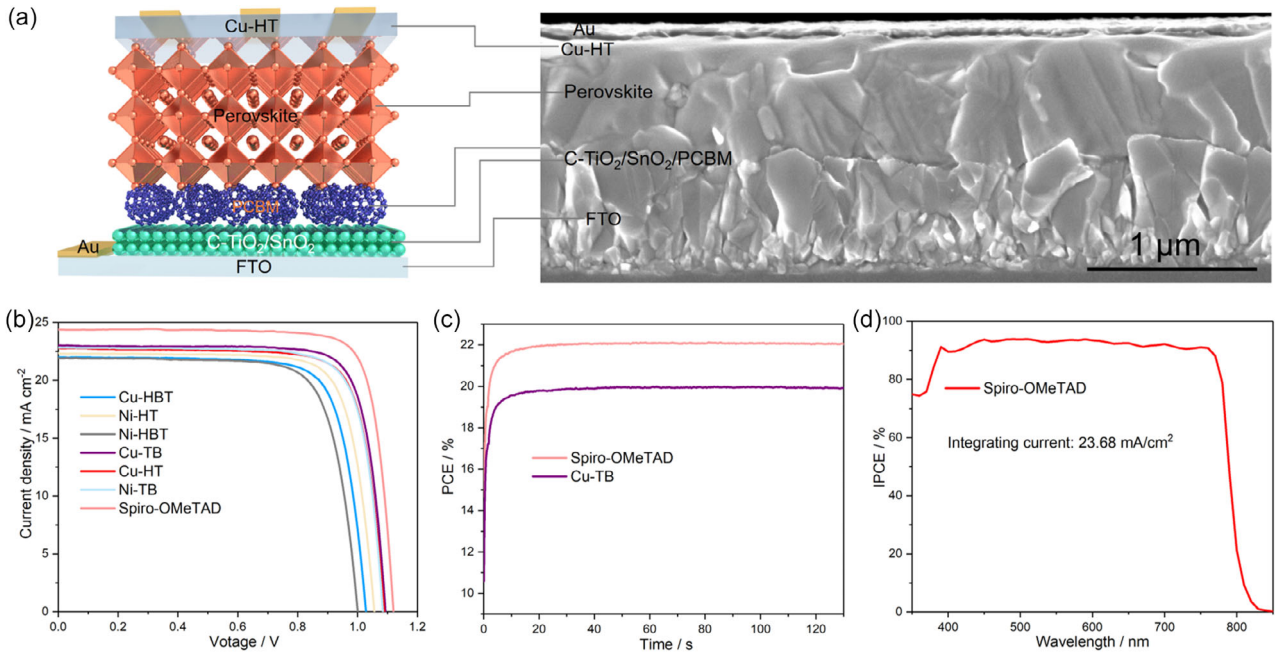

Figure 6. a) Illustration of the structure of (n-i-p) PSCs and the corresponding cross-section SEM of the device based on the **HT-CuPc** HTM. b) $J-V$ curves of the devices using the different HTMs. c) The stabilized PCE under constant exposure of 1.5 AM light for spiro-OMeTAD- and **TB-CuPc**-based devices. d) IPCE spectrum of the devices based on spiro-OMeTAD.

Table 3. Photovoltaic parameters of the (n–i–p) PSCs based on spiro-OMeTAD and the proposed MPcs.

HTMs	J_{sc} [mA cm^{-2}]	V_{oc} [V]	FF	PCE [%]
TB-CuPc	23.01	1.094	0.793	19.96
HT-CuPc	22.77	1.090	0.784	19.45
HBT-CuPc	21.97	1.027	0.769	17.35
TB-NiPc	22.82	1.084	0.786	19.44
HT-NiPc	22.34	1.055	0.776	18.28
HBT-NiPc	21.90	0.999	0.761	16.64
Spiro-OMeTAD	24.37	1.121	0.808	22.07

When bithiophene groups are attached to the Pc core, the V_{oc} of **HBT-CuPc** and **HBT-NiPc** further decreased to 1.027 and 0.999 V, respectively, and lower PCEs are observed (17.35 and 16.64%). Again, these V_{oc} losses are consistent with the HOMO destabilization resulting from the additional thiophene ring, leading to an energy mismatching with the perovskite energy levels, which is expected to increase the interface carrier recombination loss. This, together with the lower hole mobility recorded for **HT-MPc** and **HBT-MPc** containing thiophene rings, results in poorer performance for these HTMs, which is in sharp contrast to the trend previously observed.[26] However, it is important to note that the HTMs reported herein largely outperformed the Zn-based analogs, thus underscoring the key role of the metal hosted in the inner cavity of the macrocycle. Also noteworthy is that both **TB-CuPc** and **TB-NiPc** deliver PCEs well above 19%, comparable to the highest reported values for Pcs in PSCs. Despite this notable performance, our Pc-based devices are still slightly outperformed by the reference device including the archetypical spiro-OMeTAD (22.07%). This better performance mainly arises from gains in the J_{sc} and V_{oc} values, which likely result from the more suitable HOMO-LUMO energy levels of spiro-OMeTAD, as well as its transparency in the visible range. Gratifyingly, the efficiency of the device based on the champion **TB-CuPc** remains stable, exhibiting a stabilized PCE of 19.90% after 130 s light soaking, while the spiro-OMeTAD-based devices showed a stabilized PCE of 22.02% (Figure 6c). The incident photon-to-current efficiency (IPCE) of the devices using spiro-OMeTAD and our champion Pc-based HTM (Figure 6d and S14, Supporting Information) corresponds to 23.68 and 21.30 mA cm^{-2} integrated currents, which is consistent with the J_{sc} values (Table 3), confirming the accuracy of the current of J–V curves. Importantly, these devices showed negligible hysteresis (**Table 4** and **Figure 7**).

Stability notions are crucial for the commercial application of PSCs. Therefore, given the excellent performance of our CuPc-based devices, we conducted stability tests under maximum

Table 4. Photovoltaic parameters obtained from the J–V curve hysteresis of PSCs based on Spiro-OMeTAD and TB-CuPc.

HTMs	Scan direction	J_{sc} [mA cm^{-2}]	V_{oc} [V]	FF	PCE [%]
TB-CuPc	Forward	23.01	1.094	0.793	19.96
TB-CuPc	Reverse	23.04	1.063	0.773	18.93
Spiro-OMeTAD	Forward	24.37	1.121	0.808	22.07
Spiro-OMeTAD	Reverse	24.41	1.105	0.798	21.52

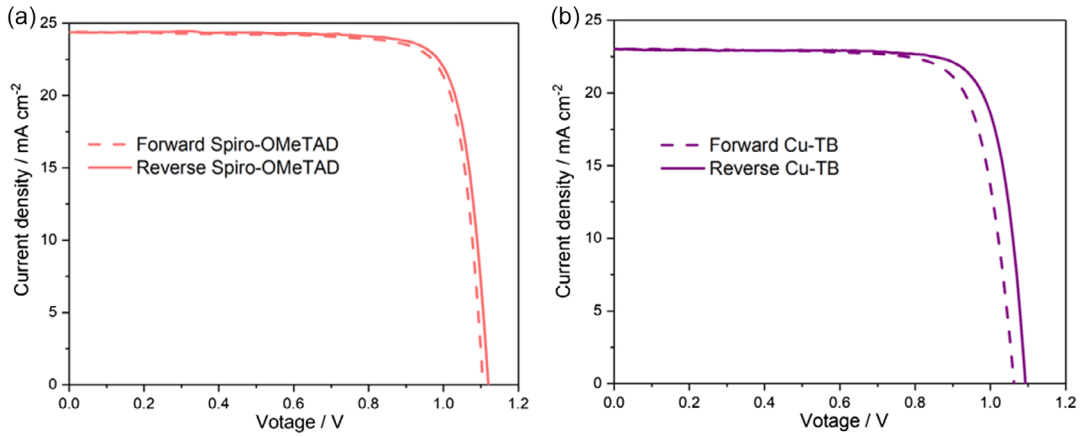

Figure 7. a) $J-V$ curve hysteresis of PSCs based on spiro-OMeTAD and b) **TB-CuPc**.

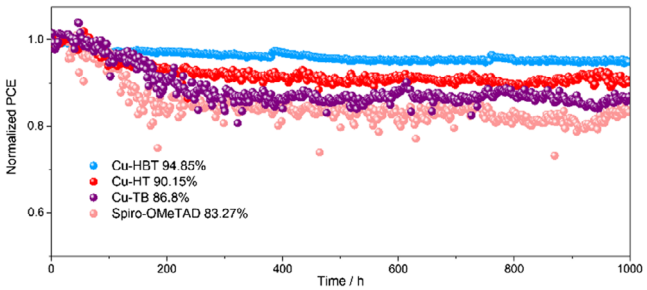

Figure 8. MPP stability of PSCs for CuPcs under the N_2 storage condition (25 °C).

power point (MPP) continuous outputting (N_2, 25 °C) conditions (**Figure 8**). Devices containing spiro-OMeTAD were also tested for comparison. In terms of MPP stability, devices based on **TB-CuPc** retained 86.8% of the initial efficiency after 1000 h of continuous outputting, higher than devices based on spiro-OMeTAD (83.27%). When one thiophene group replaced the tertbutyl substituted derivatives, the devices retained 90.15% of the initial efficiency after 1000 h of continuous outputting, indicating higher stability of PSCs based on **HT-CuPc**. This enhancement in stability may be attributed to the interaction between the sulfur (S) atom of the thiophene groups and the lead (Pb) atoms of the perovskite, as well as to the introduction of long alkyl chains. When two thiophene units are attached to the Pcs (**HBT-MPcs**), the stability of PSCs further increases to 94.85% under the same conditions. From these results, it can be concluded that the HTMs reported herein, although leading to slightly lower PCEs than spiro-OMeTAD, are largely preferred due to enhanced device stability upon their insertion. Overall, the aforementioned features render our HTMs good candidates for the realistic, efficient, and inexpensive fabrication of high-performing PSCs.

3. Conclusion

In summary, we have investigated a series of easily accessible Pcs as HTMs in mixed-ion perovskite $[FAPbI_3]_{0.85}[MAPbBr_3]_{0.15}$ solar cells, achieving PCEs well above 19%. Specifically, six different HTMs with varying peripheral groups (TB, HT, and HBT) and central metal (Cu(II) and Ni(II)) have been explored to gain insights into the structure-efficiency relationship. Remarkably, we have demonstrated, on the one hand, that Pcs hosting Cu(II) atoms generally outperform those including Ni(II) atom, and that the simplest peripheral functionalization (tertbutyl groups) leads to higher PCEs. Electrochemical measurements and DFT calculations have revealed that **TB-CuPc** presents a more stable HOMO energy level that is well aligned with the perovskite energy level, resulting in efficient charge extraction and higher V_{oc} values than their analogs. Moreover, SCLC measurements have demonstrated that **TB-CuPc** presents a superior hole mobility. Taken together, PCEs as high as 20.0% have been shown for **TB-CuPc**, which is among the highest values for Pc-based HTMs. Importantly, it has been also found that these HTMs, although leading to slightly lower PCEs than spiro-OMeTAD, significantly enhance the device stability over time, which is key for future applications. These findings will further motivate the development of readily accessible, economic, solution-processed Pc-based HMTs which, as demonstrated, hold great potential for cost-effective, realistic, and efficient energy production.

Supporting Information

Supporting Information is available from the Wiley Online Library or from the author.

Acknowledgements

J.X. and J.L. contributed equally to this work. Financial support from the Spanish MCIN/AEI (Projects PID2020-116490GB-I00, PID2020-119748GA-I00, PID2021-128569NB-I00, TED2021-131255B-C43 and C44, and CEX2019-000919-M, funded by MCIN/AEI/10.13039/501100011033 and by "ERDF A way of making Europe"), the Comunidad de Madrid (MAD2D-CM (UAM1)-MRR), and the Generalitat Valenciana (MFA/2022/017) is fully acknowledged. The MAD2D-CM (UAM1)-MRR and MFA/2022/017 projects are part of the advanced materials program supported by the MCIN with funding from the European Union NextGenerationEU (PRTR-C17.I1) and by the Comunidad de Madrid

and Generalitat Valenciana, respectively. IMDEA Nanociencia acknowledges support from the "Severo Ochoa" Programme for Centres of Excellence in R&D (MINECO, grant no. SEV2016-0686). T.T. also acknowledges the Alexander von Humboldt Foundation (Germany) for the A. v. Humboldt - J. C. Mutis Research Award 2023 (Ref 3.3-1231125 - ESP-GSA). J.L. acknowledges MECD, Spain, for a F.P.U. Fellowship. M.P.-E. acknowledges the PRE2021-097082 grant funded by MCIN/AEI and "ESF Investing in your future". J.X., M.K.N., and A.M.A. acknowledge Deputyship for Research & Innovation, Ministry of Education in Saudi Arabia, project no. 526 and 425.

Conflict of Interest

The authors declare no conflict of interest.

Data Availability Statement

The data that support the findings of this study are available from the corresponding author upon reasonable request.

Keywords

hole-transporting materials, perovskite solar cells, photovoltaics, phthalocyanines

Received: May 18, 2024
Revised: July 3, 2024
Published online: July 17, 2024

[1] J. Y. Kim, J. Lee, H. S. Jung, H. Shin, N. Park, *Chem. Rev.* **2020**, *120*, 7867.
[2] J. H. Heo, S. H. Im, J. H. Noh, T. N. Mandal, C. Lim, J. A. Chang, Y. H. Lee, H. Kim, A. Sarkar, M. K. Nazeeruddin, M. Graetzel, S. I. Seok, *Nat. Photonics* **2013**, *7*, 486.
[3] R. Sharma, A. Sharma, S. Agarwal, M. S. Dhaka, *Sol. Energy* **2022**, *244*, 516.
[4] X. Lin, D. Cui, X. Luo, C. Zhang, Q. Han, Y. Wang, L. Han, *Energy Environ. Sci.* **2020**, *13*, 3823.
[5] https://www.nrel.gov/pv/cell-efficiency.html (accessed: January 2024).
[6] H. Lu, A. Krishna, S. M. Zakeeruddin, M. Gratzel, A. Hagfeldt, *iScience* **2020**, *23*, 101359.
[7] S. S. Mali, C. K. Hong, *Nanoscale* **2016**, *8*, 10528.
[8] M. Vasilopoulou, A. Fakharuddin, A. G. Coutsolelos, P. Falaras, P. Argitis, A. R. b. M. Yusoff, M. K. Nazeeruddin, *Chem. Soc. Rev.* **2020**, *49*, 4496.
[9] M. Grätzel, *Acc. Chem. Res.* **2017**, *50*, 487.
[10] J. Urieta-Mora, I. García-Benito, A. Molina-Ontoria, N. Martín, *Chem. Soc. Rev.* **2018**, *47*, 8541.
[11] N. Ahn, D. Son, I. Jang, S. M. Kang, M. Choi, N. Park, *J. Am. Chem. Soc.* **2015**, *137*, 8696.
[12] W. S. Yang, J. H. Noh, N. J. Jeon, Y. C. Kim, S. Ryu, J. Seo, S. I. Seok, *Science* **2015**, *348*, 1234.
[13] N. Kobayashi, *100 - Synthesis and Spectroscopic Properties of Phthalocyanine Analogs*, Academic Press, Amsterdam **2003**, pp. 161–262.
[14] G. de la Torre, G. Bottari, T. Torres, *Adv. Energy Mater.* **2017**, *7*, 1601700.
[15] G. de la Torre, C. G. Claessens, T. Torres, *Chem. Commun.* **2007**, 2000.
[16] M. G. Walter, A. B. Rudine, C. C. Wamser, *J. Porphyrins Phthalocyanines* **2010**, *14*, 759.
[17] C. G. Claessens, U. Hahn, T. Torres, *Chem. Rec.* **2008**, *8*, 75.
[18] M. Urbani, M. Ragoussi, M. K. Nazeeruddin, T. Torres, *Coord. Chem. Rev.* **2019**, *381*, 1.
[19] I. Kim, H. M. Haverinen, Z. Wang, S. Madakuni, Y. Kim, J. Li, G. E. Jabbour, *Chem. Mater.* **2009**, *21*, 4256.
[20] M. Urbani, G. de la Torre, M. K. Nazeeruddin, T. Torres, *Chem. Soc. Rev.* **2019**, *48*, 2738.
[21] K. Chen, M. Cao, Y. Lin, J. Fu, H. Liao, Y. Zhou, H. Li, X. Qiu, J. Hu, X. Zheng, M. Shakouri, Q. Xiao, Y. Hu, J. Li, J. Liu, E. Cortés, M. Liu, *Adv. Funct. Mater.* **2022**, *32*, 2111322.
[22] L. D. Rollmann, R. T. Iwamoto, *J. Am. Chem. Soc.* **1968**, *90*, 1455.
[23] F. Evangelista, V. Carravetta, G. Stefani, B. Jansik, M. Alagia, S. Stranges, A. Ruocco, *J. Chem. Phys.* **2007**, *126*, 124709.
[24] T. Hung, Y. Godinez-Loyola, M. Steinbrecher, B. Kiraly, A. A. Khajetoorians, N. L. Doltsinis, C. A. Strassert, D. Wegner, *J. Am. Chem. Soc.* **2024**, *146*, 8858.
[25] S. M. Reda, *Sol. Energy* **2007**, *81*, 755.
[26] K. T. Cho, O. Trukhina, C. Roldán-Carmona, M. Ince, P. Gratia, G. Grancini, P. Gao, T. Marszalek, W. Pisula, P. Y. Reddy, T. Torres, M. K. Nazeeruddin, *Adv. Energy Mater.* **2017**, *7*, 1601733.
[27] S. Wang, T. Sakurai, W. Wen, Y. Qi, *Adv. Mater. Interfaces* **2018**, *5*, 1800260.
[28] Q. Zhang, K. Williams, J. Tatum, F. Han, X. Zhu, Q. Dai, *J. Renewable Sustainable Energy* **2021**, *13*, 063501.
[29] Z. Shuai, W. Li, J. Ren, Y. Jiang, H. Geng, *J. Chem. Phys.* **2020**, *153*, 080902.
[30] D. P. Hagberg, J. H. Yum, H. Lee, F. De Angelis, T. Marinado, K. M. Karlsson, R. Humphry-Baker, L. Sun, A. Hagfeldt, M. Grätzel, M. K. Nazeeruddin, *J. Am. Chem. Soc.* **2008**, *130*, 6259.

